

Tissue Characterization in Intravascular Ultrasound Images

Xiangmin Zhang, Charles R. McKay, and Milan Sonka,* *Member, IEEE*

Abstract—Intravascular ultrasound (IVUS) imaging permits direct visualization of vascular pathology. It has been used to evaluate lumen and plaque in coronary arteries and its clinical significance for guidance of coronary interventions is increasingly recognized. Conventional manual evaluation is tedious and time-consuming. This paper describes a highly automated approach to segmentation of coronary wall and plaque, and determination of plaque composition in individual IVUS images and pullback image sequences. The determined regions of plaque were classified in one of three classes: soft plaque, hard plaque, or hard plaque shadow. The method's performance was assessed *in vitro* and *in vivo* in comparison with observer-defined independent standards. In the analyzed images and image sequences, the mean border positioning error of the wall and plaque borders ranged from 0.13–0.17 mm. Plaque classification correctness was 90%.

Index Terms—Intravascular, plaque composition, plaque morphology, segmentation, tissue characterization, ultrasound.

I. INTRODUCTION

HEART attack and stroke are the major causes of human death, almost twice as many people die from cardiovascular diseases than from all forms of cancer combined. A number of imaging modalities exist to help diagnose coronary artery disease. Among them, X-ray coronary angiography and intravascular ultrasound (IVUS) represent the most commonly used diagnostic tools. Selective coronary angiography provides projectional X-ray images of contrast-filled coronary vessels and has been clinically used for several decades. While it provides detailed images of vessel lumen, it offers no information about the coronary wall. Intravascular ultrasound is a relatively new technique that offers image information that is complementary to that provided by angiography. The IVUS imaging (Fig. 1) generates cross-sectional images of the lumen, plaque, and vessel wall. Consequently, it facilitates analysis of atherosclerotic plaque composition.

Manuscript received December 2, 1997; revised October 1, 1998. This work was supported in part by the American Heart Association, Iowa Affiliate under Grants IA-94-GS-65 and IA-96-GS-42, and by the American Heart Association under Grant 901221. The Associate Editor responsible for coordinating the review of this paper and recommending its publication was C. Meyer. Asterisk indicates corresponding author.

X. Zhang was with the Department of Electrical and Computer Engineering, The University of Iowa, Iowa City, IA 52242 USA. He is now with Boston Scientific Corporation, San Jose, CA 95134 USA.

C. R. McKay is with the Department of Internal Medicine, The University of Iowa, Iowa City, IA 52242 USA.

*M. Sonka is with the Department of Electrical and Computer Engineering, The University of Iowa, Iowa City, IA 52242 USA (e-mail: milan-sonka@uiowa.edu).

Publisher Item Identifier S 0278-0062(98)09751-1.

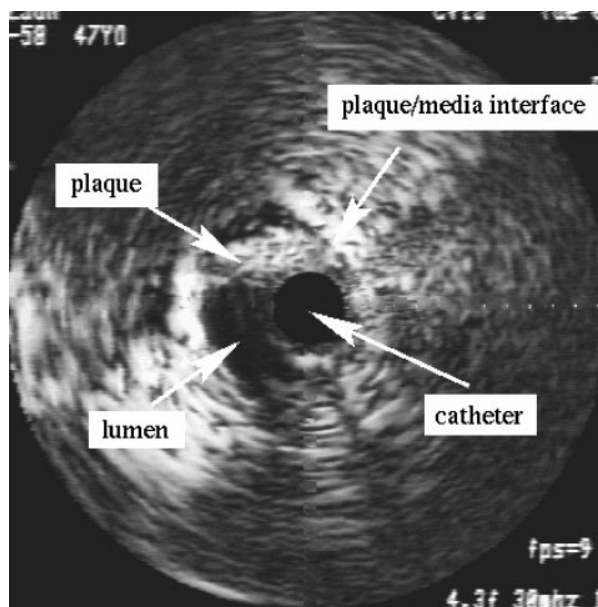


Fig. 1. Intravascular ultrasound image.

Growing evidence exists suggesting that the structure and composition of atherosclerotic plaque play important roles in coronary artery disease and in the outcomes of coronary interventions. The ability to visually identify the morphology of atherosclerotic plaque has increased the usage of intravascular ultrasound during and/or after therapeutic interventions such as balloon angioplasty, directional atherectomy and stent placement. Intravascular ultrasound findings may give rise to a modification of the treatment strategy. Lesion eccentricity and the presence or absence of calcium and its superficial or deep location in the atherosclerotic plaque demonstrated by IVUS imaging have major implications in the choice of an intervention device [1], [2].

However, visual evaluation and characterization of plaque requires integration of complex information from a large number of images and suffers from substantial inter- and intraobserver variability. Improvements in intravascular ultrasound imaging have increased the clinical utility and feasibility of the three-dimensional (3-D) quantitative analysis of the coronary wall and plaque. Three-dimensional analysis requires processing of long image sequences acquired during catheter pullback. The pullback sequence consists of a series of cross-sectional images acquired by manually or mechanically pulling the catheter back along the vessel segment. Constant pullback

speed is preferred, 1 or 0.5 mm/s is typically used. With 30 frames/s, pullback image sequences consist of hundreds of IVUS frames. Manual border identification in such image sequences is tedious and impractical for clinical use. Automated analysis is needed to bring quantitative 3-D analysis of IVUS pullback image data to routine clinical utility [3]–[11].

Several techniques for 3-D segmentation of coronary wall and plaque from IVUS image sequences evolved over the last few years [12]. One of the most widely reported semi-automated segmentation approaches that was used in clinical research was developed by Li *et al.* [8], [13], [14]. Their method is based on semi-automated segmentation of longitudinally resampled IVUS image sequences followed by lumen and media border detection in cross-sectional IVUS images. Optimal border detection approach based on dynamic programming is used. Another semi-automated method for 3-D IVUS segmentation was developed by Dhawale and colleagues [6], [15]. Again, they used dynamic programming for border detection. Meier *et al.* recently reported a 3-D IVUS segmentation approach that uses a combination of region growing and cost-function optimization [11]. Another IVUS segmentation technique based on optimal graph searching was developed by our group [16], [17]. The clinical utility of 3-D coronary vessel morphometrics for diagnosis of vascular disease, assessment of stent deployment, endoluminal grafts, results of other coronary interventions, and prediction of plaque fracture locations is discussed in [7], [9], [12], [14], [18]. All the above mentioned methods reconstruct the coronary vessels as straight pipes. Recently, the importance of geometrically correct 3-D reconstruction of coronary vessels and the associated plaque morphometrics was addressed [19]. IVUS reconstruction methods that use fusion of image data from biplane angiography and intravascular ultrasound are beginning to appear [20]–[23].

In addition to plaque morphometry, plaque composition was shown to correlate with clinical variables in atherosclerotic coronary artery disease [24], [25]. Mintz studied the role of calcium within the plaque burden [24]. Rasheed classified plaque regions as soft or hard and studied their relationship with patient-related clinical variables [25]; quantitative gray-level statistics were used for computer-assisted assessment of plaque characterization [26]. It was demonstrated in comparison with histology that IVUS images can be used for reliable visual assessment of plaque composition in regions of soft (cellular), hard (fibrocalcific), and calcified plaque [26]–[30].

Wilson and later Bridal demonstrated that there is correlation between ultrasonic attenuation and constituents of atherosclerotic plaque [31], [32]. Ultrasonic assessment of plaque composition is of direct interest in the cardiovascular research in general. Examples include ultrasonic studies of plaque morphometry and composition in carotid arteries [33]–[36].

Despite the unquestionable clinical utility of IVUS imaging, estimates of vessel morphometry and plaque characteristics continue to be made visually. Such estimates are often based on an arbitrary selected IVUS frame representing a single vessel cross section. Only a limited number of computer-aided plaque characterization methods have been published.

Picano *et al.* showed that biochemical plaque composition can be determined from ultrasound images in conventional video format [29]. Rasheed *et al.* developed a computerized method for two-dimensional (2-D) (single-frame) plaque classification *in vivo* and validated the method against histologic analysis of tissue from coronary atherectomy [26]. While the approach showed good agreement with visual and histologic assessment of plaque composition, plaque characterization was based exclusively on gray level distribution of the IVUS images and did not offer any volumetric information. As stated in [37], *analysis of the composition rather than the luminal encroachment of an atheroma is a new avenue of research available to intravascular ultrasound techniques with potential revolutionary repercussions*. Therefore, the goal of the presented work was to develop and validate a practical automated method for assessing 3-D vessel morphometry and plaque composition and to evaluate its accuracy and potential utility.

II. SEGMENTATION OF IVUS PULLBACK SEQUENCES

Our previously reported segmentation method reported in [16] automatically identified the media/adventitia border (wall border) and the plaque/lumen borders (plaque border) using a single interactively defined region of interest (ROI) in *individual* IVUS images. Two key aspects of our approach were as follows.

- Graph searching was utilized to identify globally optimal borders.
- *A priori* information was incorporated into the border detection process through the computation of local cost values. In particular, to identify the position of the wall borders, the method searched for edge triplets representing the leading and trailing edges of the laminae echoes. The interactively defined elliptical shape of the ROI served as a model of the preferred vessel shape. Knowledge of the vessel wall thickness was also used to constrain the search for the wall borders.

To facilitate an automated analysis of IVUS pullback image sequences, the ROI in which the borders are determined must be automatically identified. Then, the 3-D border detection may be performed as an extension of the border detection in individual IVUS images.

A 3-D border detection algorithm was designed that in addition to *a priori* information about 3-D coronary anatomy and ultrasound physics also uses contextual information to estimate ROI size and position changes in the successive frames. The general steps of the 3-D IVUS segmentation algorithm are shown in Fig. 2. A single elliptical ROI is interactively identified in the first image of the pullback sequence. Inside the ROI, wall, and plaque borders are automatically identified using the previously reported segmentation approach [16]. In subsequent images, current ROI's are automatically determined from the computer-detected borders in the preceding image frames.

Details of the ROI determination in successive frames are described using the following definitions.

- 1) *Fitted Ellipse*: Let A_1 and B_1 be such two points on a closed contour \mathbf{C} that have the largest mutual distance

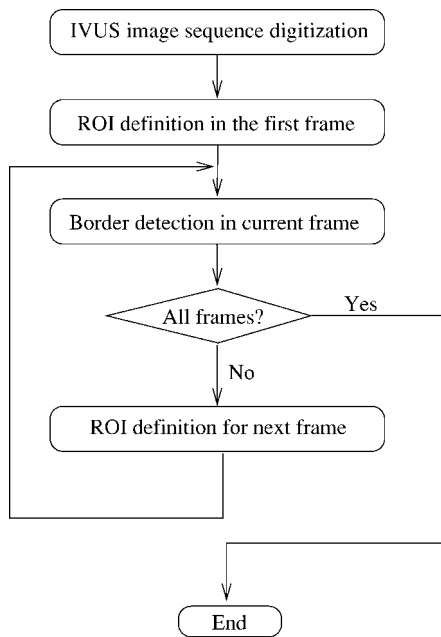


Fig. 2. Automated segmentation of intravascular ultrasound pullback image sequences.

of all point pairs of the closed contour C . Let A_2B_2 be a line perpendicular to A_1B_1 that divides A_1B_1 in two parts of equal length, $A_2, B_2 \in C$. The fitted ellipse of C is then defined as an ellipse with long axis being A_1B_1 and the length of its short axis equal to the length of A_2B_2 [Fig. 3(a)].

- 2) *Average Distance Between Two Contours*: Let the point $Q_i \in C_2$ be the closest point for the point $P_i \in C_1$. Let the distance between P_i and Q_i be denoted by d_i . The average distance between two contours C_1 and C_2 is defined as the mean distance $d_{mean} = \sum_i d_i/n$ where n is the number of contour points of the contour C_1 [Fig. 3(b)].
- 3) *Contour Expanding or Shrinking*: Let a new contour C' consisting of points P' result from expanding (shrinking) of a contour C consisting of points P . Let the amount of expanding (shrinking) be defined by a distance d . Each contour point $P'_i \in C'$ is defined as being located on a normal to the contour C at the point $P_i \in C$ for which the distance $P_iP'_i = d$ and the points P'_i are located outside (inside) of the contour C [Fig. 3(c)].

Let the currently analyzed frame of the IVUS pullback image sequence be denoted by $n - 1$, let the previous frame be denoted by $n - 2$, and let the frame to be analyzed next be denoted by n . Then, the outside limit of the elliptic ROI in the next frame n is estimated using the following steps.

- 1) Following the definition of a fitted ellipse, fit an ellipse E_f to the wall border that was determined in the frame $n - 1$.
- 2) Determine the average distance d between the contour E_{n-1} identifying the outside limit of the elliptic ROI in the frame $n - 1$ and the ellipse E_f .
- 3) Expand the ellipse E_f by the distance d to define an ellipse E'_{n-1} .

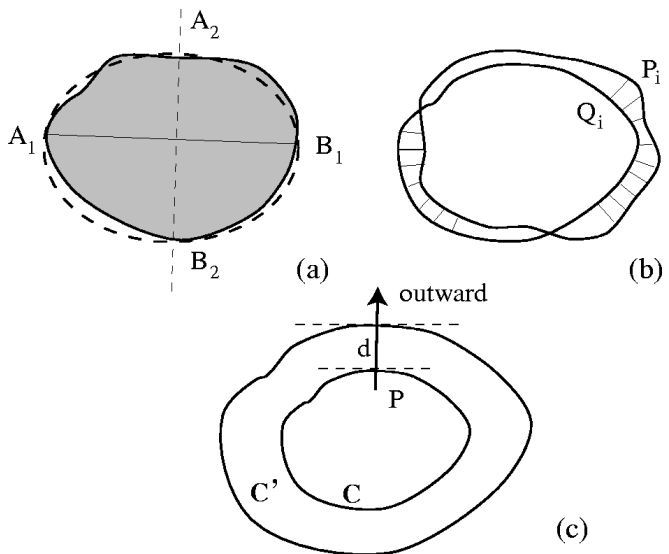


Fig. 3. ROI determination in successive frames (a) Fitting an ellipse to a closed contour. (b) Averaging two closed contours. (c) Contour expansion by d .

- 4) Compute the weighted averages l and s of the long and short axis length, respectively, of the ellipse E'_{n-2} (the outside ROI ellipse in the frame $n - 2$), E_{n-1} , and E'_{n-1}

$$l = w_1 l_{n-2} + w_2 l_{n-1} + w_3 l'_{n-1} \quad (1)$$

$$s = w_1 s_{n-2} + w_2 s_{n-1} + w_3 s'_{n-1} \quad (2)$$

where l_m, s_m denote long and short axis lengths of the respective ellipses. The weights w_i represent the parameters of the algorithm.

- 5) Adjust the ellipse E_f so that the lengths of its axes are of the lengths l and s , respectively. Let the new adjusted ellipse be denoted by E_n . The new elliptic ROI in the frame n is defined by the ellipse E_n .

A heavily smoothed and shrunk plaque border P_{n-1} previously determined in frame $n - 1$ is used to define the inside limit of the ROI in frame n . During the segmentation process, the elliptical ROI's were monitored by an observer to ensure the vessel wall cross sections were included within the predicted ROI. If the ROI failed to enclose the vessel wall, the segmentation process was interrupted, the ROI was adjusted interactively and segmentation was restarted.

III. TISSUE CHARACTERIZATION IN IVUS IMAGES

In addition to the 3-D plaque morphometry that can be determined from segmented IVUS pullback image sequences, determination of plaque composition is of high clinical importance. The ultrasonic appearance of the atherosclerotic plaque depends on its composition [26], [30], [37]. The following sections describe a newly developed automated texture-based method for plaque composition assessment.

A. Ultrasonic Appearance of Wall and Plaque

High-frequency (20–30 MHz) ultrasonography allows imaging of relatively small structures (<0.2 mm). The bright reflection of ultrasound at a tissue interface depends on the

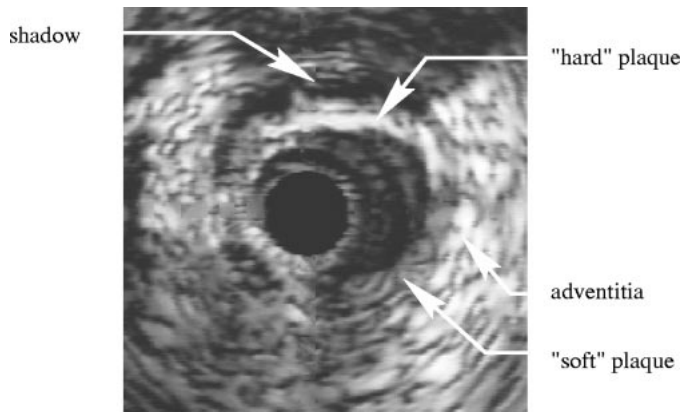


Fig. 4. Ultrasonic appearance of wall and plaque.

angle of the beam to the reflector and the acoustic impedance mismatch between the two adjacent tissues. In general, the structural components of the elastic artery consist of a highly organized arrangement of lamellae. The lamellae consist of repeating modules of elastin, collagen, and smooth muscle cells, which decrease ultrasound penetration. An overview of the potential utility and limitations of IVUS for quantitative characterization of vascular tissue can be found in [38].

Among all the components, the adventitia normally produces the highest gray level intensity. Characteristic gray level appearances of other tissue types have been defined with their relative brightness compared to that of the adventitia. The goal is to distinguish between regions of soft plaque (lipids, cellular components, loose connective tissue) and hard plaque (dense fibrous tissue, collagen, elastic fibers, proteoglycan, necrotic debris with or without calcification) [37]. These two groups were previously shown to be visually distinguishable by experienced human observers in comparison to histology [39].

- Hard plaques are composed of fibrous tissue often in complex layers. In IVUS images, hard plaques are highly reflective of ultrasound and produce bright echoes similar to the adventitia (Fig. 4). Calcified hard plaque regions are typically identified by high-amplitude echo signals with complete distal shadowing. Consequently, hard plaque regions are characterized in IVUS images as texturally heterogeneous, high contrast regions located inside of thick plaque that contain very bright echoes and are often trailed by shadowed areas. (Note that the textural image heterogeneity does not necessarily correlate with tissue heterogeneity.)
- Soft plaques usually consist of highly cellular areas of intimal hyperplasia and often contain cholesterol, thrombus, and loose connective tissue types. Ultrasound images of soft plaque are characterized by weaker and more texturally homogeneous echoes and show low contrast (Fig. 4).

If the hard plaque is calcified, the composition of the shadowed region behind the calcified plaque is not depicted on the IVUS image. Therefore, shadows behind the calcified hard plaque form a third class. An example of observer-defined plaque composition is given in Fig. 5.



(a)



(b)

Fig. 5. Observer-defined plaque composition. (a) Original intravascular ultrasound image. (b) Manual plaque classification; soft plaque (two side regions) and hard plaque (top region).

B. Plaque Description in Elementary Regions

To assess plaque composition, plaque type is determined in narrow plaque wedges called elementary regions. Classification labels are assigned to the pixel of interest (POI) associated with each elementary region. Prior to defining the elementary regions, the entire plaque region A is straightened into a rectangular region B of a constant height H along the plaque/lumen interface (Fig. 6). The width W of the straightened region B is equal to the lengths of the plaque/lumen border. Thus, each pixel of region B is corresponding to one pixel in region A but not vice versa. This is a standard geometric image transform. While it may cause minor local gray level changes due to resampling and interpolation, it does not affect global gray level parameters.

In order for B to contain all elementary regions in the radial direction, maximum thickness t_{\max} of the plaque region A is computed first. Then, the height of the region B is determined as

$$H = t_{\max} + h \quad (3)$$

where h is the constant height of all elementary regions. The straightened rectangular region B thus contains all plaque, and may include some portions of the wall and adventitia. Each

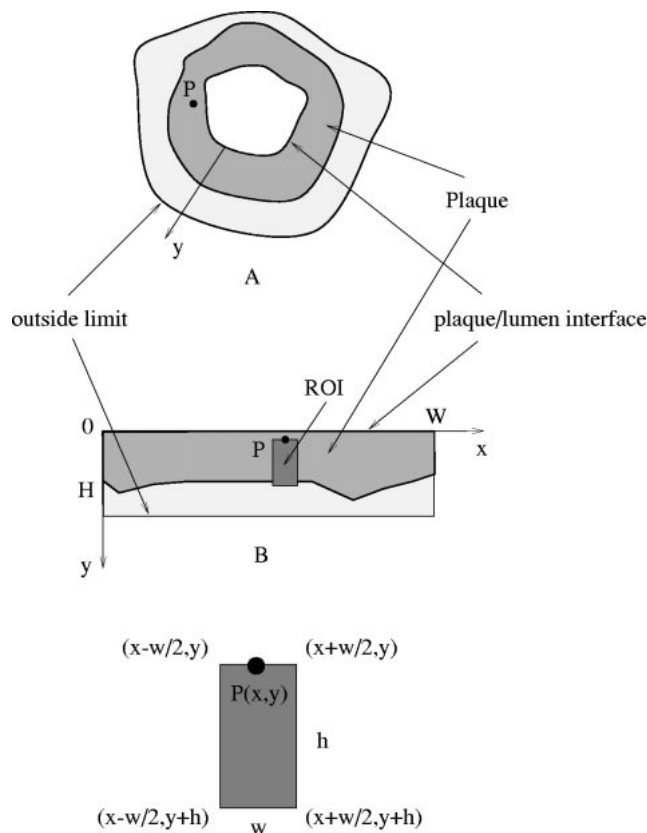


Fig. 6. Plaque region straightened along the plaque border. Original plaque region *A*, straightened plaque region *B*, point of interest *P* and its elementary region (bottom, enlarged).

pixel in *B* is a POI candidate and one and only one POI is selected in each column (along direction *y* in Fig. 6). To become a POI, the candidate pixel must belong to the plaque region and have the highest intensity level of the plaque region in this column as described below.

The elementary region associated with the point of interest $P(x, y)$ is defined as a wedge (a rectangle in the straightened image), the upper left and lower right corners of which are $(x-w/2, y)$ and $(x+w/2, y+h)$, where w and h are the width and height of the elementary region, respectively (Fig. 6). Only one elementary region is defined for every column in the straightened rectangular region. Adjacent elementary regions overlap by $w - 1$ pixels.

Plaque wedges may contain a mixture of soft and hard plaque. Consequently, for each wedge containing hard plaque, the plaque wedge may appear as a two- or three-layered structure along the *y* direction: hard plaque/shadow, or soft plaque/hard plaque/shadow. The rationale for defining the point of interest as the pixel associated with the brightest plaque location along the *y* direction is to maximize the homogeneity of the elementary plaque region. Thus, soft plaque tissue located closer to the lumen/plaque border than the hard plaque is excluded from the elementary region since it does not belong to hard plaque region and consequently has different texture appearance. Therefore, elementary regions are positioned in the plaque wedge along the *y* axis to start at the point with the maximum gray level of the plaque in order to enhance sensitivity of the employed texture descriptors.

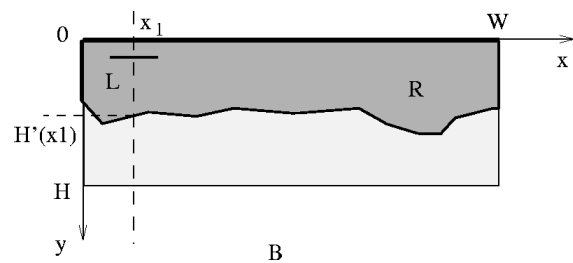


Fig. 7. Searching for elementary regions inside of the plaque region.

To determine the POI and the elementary region for each plaque wedge, a horizontal line segment *L* of the same width w as the elementary regions is moving inside of the region *B* (Fig. 7). When searching for the elementary region at column x_1 , the line segment *L* is initially placed centered at $(x_1, 0)$ and moves vertically along the *y* direction. Gray levels of pixels are averaged along the line segment *L*, $M(x_1, y)$ represents the mean gray values

$$M(x_1, y) = \frac{1}{w} \sum_{i=-w/2}^{w/2} I(x_1 + i, y). \quad (4)$$

Then, the y_1 coordinate of the point of interest $P(x_1, y_1)$ associated with the column x_1 is determined to satisfy the following equation

$$E(x_1, y_1) = \max_{0 \leq y \leq H'(x_1)} M(x_1, y) \quad (5)$$

where $H'(x_1)$ is the thickness of the plaque at column x_1 . The region between the plaque/lumen interface ($y = 0$) and the POI row ($y = y_1 - 1$) is excluded from the elementary region and is not used for determining quantitative plaque descriptions.

C. Texture Measurements

In the elementary regions, the following texture measures are computed to serve as features distinguishing between the hard and soft plaque. The texture descriptors were selected since they have proved useful in a variety of medical and nonmedical applications in the past [40].

1) *Gray-Level-Based Texture Descriptors*: These included standard features of *histogram contrast*, *skewness*, *kurtosis*, *dispersion*, and *variance*. In addition, a property describing the *radial profile* was designed to reflect the different gray level profile characteristics of the hard and soft plaque. For an elementary region with the POI at (x_1, y_1) (Fig. 8), the *radial profile* property can be determined as

$$\text{radial_profile} = \frac{E(x_1, y_1)}{\max_{\Delta y} E(x_1, y_1 + \Delta y)} \quad (6)$$

where $\Delta y = 10, 20, \dots, h$.

2) *Co-Occurrence Matrices*: These matrices describe repeated occurrences of some gray level configurations in the plaque texture classes. An occurrence of some gray level configuration may be described by a matrix of relative frequencies $F_{\phi, d}(a, b)$, describing how frequently two pixels with the gray levels a, b appear in the texture separated by

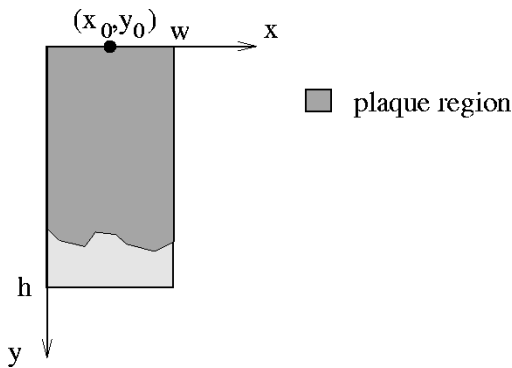


Fig. 8. Calculation of the *radial-profile* property in an elementary region.

a distance d in direction ϕ [40]. The features *energy*, *entropy*, *maximum probability*, *contrast*, and *inverse difference moment* were computed.

3) *Run-Length Measures*: These measures describe the maximum contiguous set of constant gray level pixels located at a specified direction. A large number of neighboring pixels of the same gray level represents a coarse texture, a small number of these pixels represents a fine texture and the lengths of texture primitives at different directions can serve as texture descriptors [40]–[42]. Two run-length features were computed: *short primitives emphasis* and *long primitives emphasis*.

4) *Fractal-Based Measures*: These measures are calculated through the transformation of image space to fractal dimension, *Brownian fractal dimension* was computed [43].

D. Plaque Recognition

From the large number of calculated features, correlated ones were removed. Then, features with the highest discrimination power were identified using the inter-class distance search criterion and the Euclidean metric [44]. The following three descriptors were identified as providing the best features for soft/hard plaque classification in IVUS images: radial profile, long run emphasis, and the fractal dimension. A classifier with piecewise linear discrimination functions was trained using the three selected features and used for classification. The number of exemplars defining the piecewise linear discrimination function results from the learning process. This is an iterative learning process. Initially, a small number of exemplars, possibly one, is given to each class by grouping the training samples. An exemplar is computed as the center of each group. The training set is then classified using the exemplars. If the classification is not correct, the number of exemplars is increased and the training samples regrouped. New exemplars are derived. This process is repeated until specified criteria are satisfied.

In the testing set of IVUS images, each elementary region was classified as containing soft or hard plaque. The elementary regions labeled as hard plaque were further divided into hard plaque and shadow subregions based on their gray level intensities. This was done using gray level thresholding along each row.

To suppress classification artifacts that are present in the shadow region, a 7×7 median filter is applied to the entire region.

After the plaque type classification was performed in pull-back sequences, a post-processing method was included that considered 3-D contextual information. After the classification of individual elementary regions was completed in the entire sequence, the plaque type of each pixel was determined as the majority type among the pixels of the same spatial location in the preceding three frames, the current frame, and the successive three frames.

IV. EXPERIMENTAL METHODS

A. Image Acquisition

Intravascular ultrasound images were obtained from coronary arteries *in vivo* and *in vitro*, using 2.9 French intracoronary ultrasound imaging catheters (Boston Scientific, San Jose, CA). IVUS images were recorded on S-VHS video tapes and digitized using a high-end commercially available digitizer (Parallax Xvideo 700) at image resolution of 640×480 pixels, 0.03 mm/pixel, digitization rate up to 30 frames/s.

Single-frame images were stored as JFIF format and later converted to 8-bit gray level raw data format. Image sequences were digitized using JPEG standard with highest quality provided by the digitizer and later decompressed into the raw data format.

B. Experimental Data

To validate our segmentation method in IVUS pullback image sequences, six *in vivo* IVUS pullback sequences were acquired. The speed of the catheter pullback was approximately 1 mm/s and the images were digitized at a frame rate of 30 frames/s. Each pullback sequence depicted 5–11 mm of the left anterior descending coronary artery (LAD) and contained between 150 and 330 video frames. The IVUS pullback images were acquired from patients undergoing interventional coronary treatment. Pullbacks were acquired after directional coronary atherectomy. In one of the six sequences, calcified plaque did not permit ultrasound visualization of the wall in a large portion of the sequence and this sequence was excluded from further experiments.

Pullback sequences acquired *in vivo* often contain complex cardiac motion and rapid changes of signal attenuation over time. These may cause problems for computerized border detection. Through the usage of electrocardiogram (ECG)-gated images, we were able to improve the algorithm performance substantially. In the digitized *in vivo* pullback sequences, systolic and mid-diastolic frames were selected to form ECG-gated pullback sequences. The frame selection was performed according to the accompanying ECG signal available on the IVUS frames. The ECG-gated sequences contained 5–11 frames each and were analyzed in both directions (distal to proximal and proximal to distal). Thus, the total of $5 \times 2 \times 2 = 20$ ECG-gated IVUS pullback sequences were available for the validation experiments.

To validate our plaque characterization method, 12 IVUS images from eight diseased cadaveric human hearts were digitized from video tapes. Each image contained both soft and hard plaque regions and consisted of 150–300 elementary

regions per image. First, the plaque regions in all 12 images were segmented using our border detection approach. Then, each elementary plaque region was labeled as containing soft or hard plaque. The classifier was trained on manually determined patterns of soft and hard plaque elementary regions. Nonhomogeneous elementary regions, containing a mixture of soft and hard plaque tissues, were excluded from the training set.

Due to the limited data set that was available for validation, we used the *leave-one-out*, or *Jackknife*, approach to assess classification correctness [45], [46]. First, 11 of the 12 images were selected to train the classifier. The remaining image was then used for testing the resulting classifier. The process was repeated 12 times, always using 11 images to train the classifier and the remaining image to test the classifier. This is a standard process used in pattern recognition when limited numbers of training/testing data are available. Note that the classifier did not produce a single decision per training session. Rather, 200–300 decisions were made each time since each elementary region was classified.

To demonstrate the feasibility of 3-D analysis of plaque morphometry and composition in IVUS pullback sequences, a 14-mm pullback sequence was acquired from a diseased cadaveric human heart. This IVUS pullback sequence contained 425 frames.

C. Independent Standards

To assess performance of our segmentation method in IVUS image sequences, we compared the automatically detected borders with the manually identified borders defined by an expert observer in a blinded fashion. The observer-defined borders served as an independent standard. In each IVUS sequence, the first, middle, and last frames of each ECG-gated IVUS sequence were manually traced to define the independent standard for coronary wall and plaque borders. Unlimited amount of tracing and editing was allowed.

To assess the correctness of plaque characterization, the automatically classified plaque regions were compared with the manual classification of plaque composition [Fig. 5(b)]. Soft and hard plaque regions were carefully outlined by an expert observer in a blinded fashion. A good agreement between visual plaque characterization in the two employed plaque tissue types and histology was previously demonstrated by our expert observer [39].

D. Quantitative Indexes

To compare computer-detected and observer-defined borders, we calculated lumen area as the area enclosed by the plaque border, plaque area as the area between the plaque border and the wall border, and the maximum and root-mean-square (rms) errors of border positioning by measuring the distances between corresponding boundary points. Corresponding points were defined as pairs of points, the first point being from the computer detected border and the second one from the independent standard border that were closest to each other using the Euclidean metric.

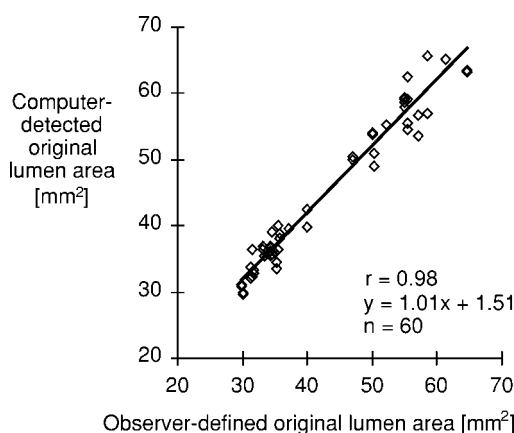


Fig. 9. Comparison of computer-detected and observer-defined lumen areas.

To assess the performance of automated plaque characterization, we determined classification correctness as the ratio of the number of correctly labeled elementary regions and the total number of elementary regions summed across all images. The classification correctness was individually determined for each plaque class as well as overall.

To evaluate the accuracy of a clinically important measure of plaque composition, the *percent circumference of hard plaque* was defined as

$$\frac{\text{circumference_of_hard_plaque}}{\text{circumference_of_plaque}} \times 100\% \quad (7)$$

where *circumference_of_hard_plaque* was expressed in degrees. The error of percent circumference of hard plaque was defined as the difference between observer-defined and computer-detected percent circumference of hard plaque.

All errors are expressed as mean \pm standard deviation. Regression equations were compared to the equation of the line of identity using *t*-statistic for the slope and intercept.

V. RESULTS

A. Three-Dimensional Image Segmentation

Our method successfully identified wall borders and plaque borders in all 20 ECG-gated IVUS pullback image sequences. After the interactive definition of the ROI in the first frames of the sequences, all borders were identified automatically and were not manually edited. A good correlation was obtained between computer-detected and observer-defined lumen and plaque areas ($r = 0.98$, $y = 1.01x + 1.51$, Fig. 9; $r = 0.94$, $y = 1.06x - 0.09$, Fig. 10). The slope and intercept of the original lumen area regression line did not differ significantly from one and zero, respectively ($p > 0.5$, $p > 0.1$). For the plaque area, the regression line slope and intercept also did not differ significantly from one and zero, respectively, ($p > 0.2$, $p > 0.9$). The computer-determined borders were quite accurate with the maximum and rms border positioning errors summarized in Table I. The maximum positioning errors mean that at any given radius, the border detection may locate the borders with errors of approximately 0.3–0.4 mm. An example of the coronary wall and plaque borders automatically

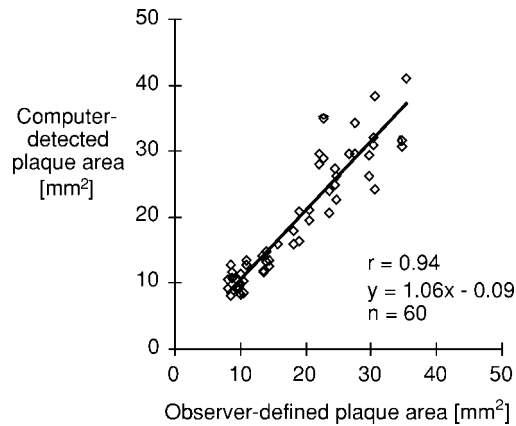


Fig. 10. Comparison of computer-detected and observer-defined plaque areas.

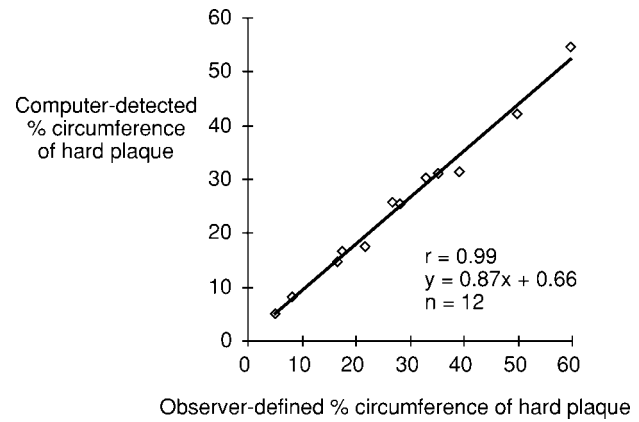


Fig. 11. Comparison of computer-detected and observer-defined percent circumference of hard plaque.

TABLE I
BORDER POSITIONING ACCURACY IN ECG-GATED PULLBACK SEQUENCES

border positioning error	maximum	rms
wall border	0.30 ± 0.13 mm	0.13 ± 0.05
plaque border	0.40 ± 0.19 mm	0.17 ± 0.08

detected in an IVUS frame of the pullback image sequence is given in Fig. 13(b).

B. Tissue Characterization

Plaque composition in the 12 images was automatically determined with classification correctness of 89.9% overall. Hard plaque was correctly classified in 89.2% of elementary regions (653/732) and soft plaque classification correctness was 90.2% (1805/2001).

A good correlation was found between the computer-detected and observer-defined percent circumference of hard plaque ($y = 0.87x + 0.66$, $r = 0.99$) (Fig. 11). The average error of percent circumference of hard plaque was $3.2\% \pm 2.7\%$. An example of automated plaque classification is given in Fig. 12.

To explore the feasibility of 3-D plaque characterization, the 14-mm cadaveric pullback sequence was first segmented using our 3-D segmentation approach. Then, plaque characterization was performed in a 101-frames-long subsequence that contained a mixture of hard and soft plaque (frames 168–268 of the original sequence). Each frame was classified using the classifier previously trained in the 12 IVUS images used for quantitative validation for which the training set was available. Vessel wall and lumen borders of the diseased cadaveric coronary artery were detected and the plaque characterized as demonstrated in Fig. 13(a)–(c). The 3-D reconstruction of the entire pullback cut in half for better visualization of the plaque composition is shown in Fig. 13(d).

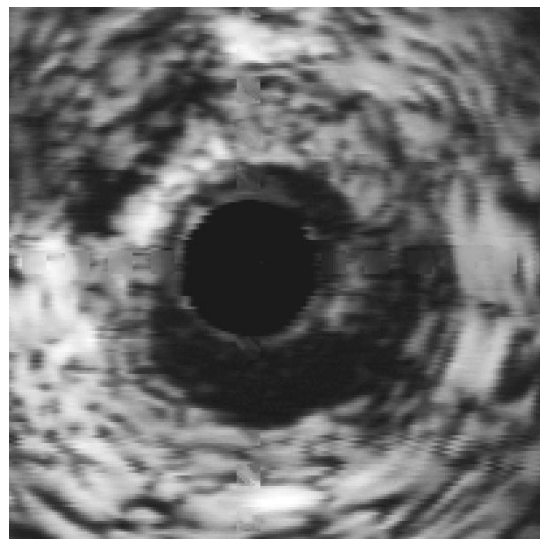
VI. DISCUSSION

Estimation of the coronary wall and plaque borders in the successive frames of the pullback sequence represents the key step to eliminate the human interaction and to develop a fully

automated IVUS sequence analysis method. Obviously, if the ROI is positioned accurately, the sequence border detection problem reduces to the border detection in an individual frame. However, with the variability of coronary cross-sectional morphology, it is often impossible to predict the ROI position accurately. In our method, it is imperative that the ROI contains the image portion in which all three borders of interest are positioned. To guarantee that the borders are included in the ROI, the ROI must increase in size compared to the size of the interactively defined ROI in individual frames. Therefore, the robustness of the border detection in individual frames is also extremely important. The more robust the method for border identification in individual frames, the less sensitive the results are to the accurate positioning of the ROI.

Considering current state-of-the-art in IVUS image segmentation, the IVUS sequences must be ECG gated to suppress the influence of the cardiac motion on the cross-sectional images and to facilitate a robust and fully automated border detection in pullback sequences. While we demonstrated that our method can be applied to non-ECG-gated IVUS pullback sequences, it may fail to correctly detect the borders in some IVUS frames due to the excessive frame-to-frame motion. The ECG gating requirement substantially decreases the method's failure rate and thus the need for manual intervention and restarting of the border detection process. As was demonstrated in the 20 ECG-gated pullback sequences that were analyzed as part of this study, no manual editing of the predicted ROI's and no restarting of the border detection process were needed. We presume that slower pullback speeds combined with ECG-gating represent the IVUS sequence acquisition method of choice if automated volumetric analysis is the goal.

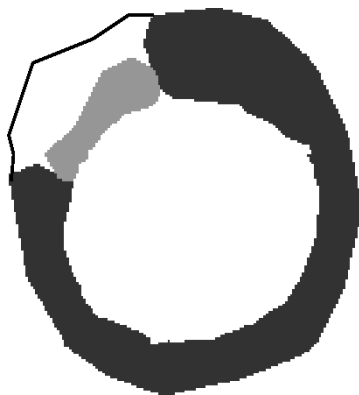
The method for automated plaque characterization presented here was developed and validated in individual IVUS image frames and its applicability was demonstrated in a 3-D pullback sequence. We expect that by combining our 3-D IVUS image segmentation method and the plaque characterization approach reported here, we will be able to develop and fully validate a method for truly 3-D plaque characterization. Additional contextual information, such as 3-D connectivity, should further improve the plaque classification results.



(a)



(b)



(c)

Fig. 12. Automated plaque characterization. (a) Original image. (b) Computer-detected soft (black), hard (gray) plaque, and shadow (white) regions, plaque borders were determined automatically. (c) Observer-identified soft, hard, and shadow plaque regions.

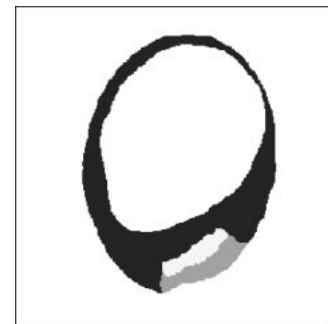
Using the currently available IVUS images, even quantitation of the total amount of vessel calcification or hard plaque volume has its limitations. Total calcium burden often cannot be estimated, because deeper structures that may or may not be calcified are hidden in the shadow of more superficially calcified regions. At the same time, brightness of the initial bright echo does not indicate the total depth or amount of



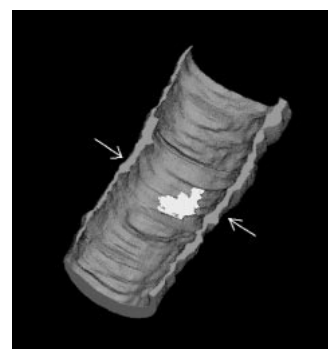
(a)



(b)



(c)



(d)

Fig. 13. A 3-D reconstruction of a coronary vessel from a 14 mm pullback sequence. (a) Original image. (b) Automated border detection. (c) Plaque composition in the IVUS frame shown in (a), soft plaque region is black, hard plaque region is light gray, hard plaque shadow is gray. (d) Plaque composition of the entire pullback sequence, hard plaque is shown as a bright region. The arrows depict the location of the IVUS frame given in panels (a)–(c).

calcification. Therefore, quantification of calcification by intravascular ultrasound can be expressed only as the arc length [37], [47]–[49]. There are additional difficulties associated

with ultrasound tissue imaging; gain setting of the IVUS device being one of them. Image brightness may also vary in fibrotic plaques due to angle dependency of echo responses with respect to ultrasound beam. While we hypothesize that our border detection and plaque characterization techniques will be able to perform well in such situations due to their primary responses to relative changes of echo intensity and not to absolute intensities, proving this hypothesis remains for future work.

On the other hand, intravascular ultrasound images facilitate detailed measurements of atherosclerotic lesions and can be used to differentiate tissue characteristics and to evaluate plaque composition. In agreement with our previous studies comparing visual analysis of plaque composition from cross-sectional IVUS images and histology [39], plaque was classified in three classes—soft, hard, and shadow in the presented study. Visual assessment of plaque type is limiting the number of classes that can be reliably distinguished by a human observer. However, plaque characterization may not necessarily be limited to classification of soft and hard plaques especially if radio-frequency (RF) data are available for computerized image analysis. Ultrasonic methods for more detailed plaque characterization can be expected in the future.

Several limitations of our work are worth noting. First, observer identification of wall and lumen morphometry inevitably suffers from interobserver and intraobserver variability and may not represent an ideal independent standard. Similarly, expert definition of plaque composition from IVUS images is irreproducible and only quantitative histology can provide an alternative independent standard. Unfortunately, when used for validation purposes in fresh cadaveric vessels, histology has associated problems with shrinkage and geometric distortions that make direct comparison of IVUS and histology a nontrivial task.

VII. CONCLUSION

Automated determination of coronary wall and plaque borders plays a very important role in visualization and quantitation of 3-D volumetric data from IVUS pullback image sequences. Although additional validation is needed in slower pullback sequences that offer larger numbers of ECG-gated images from each pullback, the presented method holds great promise for reliable, robust, and clinically applicable segmentation of IVUS pullback image sequences. The automated plaque characterization method reported here produced good assessment of plaque composition in the analyzed IVUS images. The method itself is not limited to classification of soft and hard plaque but is, in general, also applicable to more detailed plaque characterization.

Although truly accurate assessment of vessel morphometry and plaque composition can currently only be obtained using quantitative histology, our results clearly demonstrate the feasibility of automated segmentation and plaque classification in intravascular ultrasound data. The presented method holds substantial promise for segmentation and tissue characterization in 2-D and 3-D IVUS images when applied in clinical setting.

REFERENCES

- [1] G. S. Mintz, J. J. Popma, C. J. Ditrano, J. Mackenzie, and L. F. Satler, "Intravascular ultrasound vs. quantitative coronary angiography: A statistical comparison of 538 consecutive target lesions (abstract)," *Circ.*, vol. 88, pp. 1–411, 1993.
- [2] G. S. Mintz, A. D. Pichard, J. A. Kovach, K. M. Kent, L. F. Satler, P. J. Saturnino, J. J. Popma, and M. B. Leon, "Impact of preintervention intravascular ultrasound imaging on transcatheter treatment strategies in coronary artery disease," *Amer. Heart J.*, vol. 73, pp. 423–430, 1994.
- [3] K. Rosenfield, D. W. Losordo, K. Ramaswamy, J. O. Pastore, R. E. Langevin, S. Razvi, B. D. Kosowsky, and J. M. Isner, "Three-dimensional reconstruction of human coronary and peripheral arteries from images recorded during two-dimensional intravascular ultrasound examination," *Circ.*, vol. 84, pp. 1938–1956, 1991.
- [4] J. B. Hermiller, C. E. Buller, A. N. Tenaglia, K. B. Kisslo, H. R. Phillips, T. M. Bashore, R. S. Stack, and C. J. Davidson, "Unrecognized left main coronary artery disease in patients undergoing interventional procedures," *Amer. J. Cardiol.*, vol. 71, pp. 173–176, 1993.
- [5] J. R. T. C. Roelandt, F. J. T. Cate, W. B. Vletter, and M. A. Taams, "Ultrasonic dynamic three-dimensional visualization of the heart using a vario-plane transesophageal imaging transducer (Varioplane Echo-CT)," *J. Amer. Soc. Echocardiogr.*, vol. 7, pp. 217–229, 1994.
- [6] P. J. Dhawale, D. L. Wilson, and J. M. Hodgson, "Volumetric intracoronary ultrasound: Methods and validation," *Cathet. Cardiovasc. Diagn.*, vol. 33, pp. 296–307, 1994.
- [7] D. B. Reid, M. Douglas, and E. B. Diethrich, "The clinical value of three-dimensional intravascular ultrasound imaging," *J. Endovasc. Surg.*, vol. 2, pp. 356–364, 1995.
- [8] C. von Birgelen, C. D. Mario, W. Li, J. C. Schuurbers, C. J. Slager, P. J. de Feyter, J. R. Roelandt, and P. W. Serruys, "Morphometric analysis in three-dimensional intracoronary ultrasound: An *in vitro* and *in vivo* study performed with a novel system for the contour detection of lumen and plaque," *Amer. Heart J.*, vol. 132, pp. 516–527, 1996.
- [9] R. Gil, C. von Birgelen, F. Prati, C. D. Mario, J. Ligthart, and P. W. Serruys, "Usefulness of three-dimensional reconstruction for interpretation and quantitative analysis of intracoronary ultrasound during stent deployment," *Amer. J. Cardiol.*, vol. 77, pp. 761–764, 1996.
- [10] J. H. C. Reiber and E. E. van der Wall, *Cardiovascular Imaging*. Dordrecht, The Netherlands: Kluwer Academic, 1996.
- [11] D. S. Meier, R. M. Cothren, D. G. Vince, and J. F. Cornhill, "Automated morphometry of coronary arteries with digital image analysis of intravascular ultrasound," *Amer. Heart J.*, vol. 133, pp. 681–690, 1997.
- [12] M. Sonka, C. R. McKay, and C. von Birgelen, "Computer analysis of intravascular ultrasound images," in *Medical Imaging Techniques and Applications*, C. T. Leondes, Ed. Amsterdam, The Netherlands: Gordon and Breach, 1997, pp. 183–226.
- [13] W. Li, E. J. Gussenhoven, Y. Zhong, S. H. K. The, C. D. Mario, S. Madretsma, F. van Egmond, P. J. de Feyter, H. Pieterman, H. van Urk, H. Rijsterborgh, and N. Bom, "Validation of quantitative analysis of intravascular ultrasound images," *Int. J. Cardiac Imag.*, vol. 6, pp. 247–254, 1991.
- [14] C. von Birgelen, G. S. Mintz, A. Nicosia, D. P. Foley, W. J. van der Giessen, N. Bruining, S. G. Airriian, J. R. T. C. Roelandt, P. J. de Feyter, and P. W. Serruys, "Electrocardiogram-gated intravascular ultrasound image acquisition after coronary stent deployment facilitates on-line three-dimensional reconstruction and automated lumen quantification," *J. Amer. Coll. Cardiol.*, vol. 30, pp. 436–443, 1997.
- [15] P. J. Dhawale, D. L. Wilson, and J. M. Hodgson, "Optimal data acquisition for volumetric intracoronary ultrasound," *Cathet. Cardiovasc. Diagn.*, vol. 32, pp. 288–299, 1994.
- [16] M. Sonka, X. Zhang, M. Siebes, M. S. Bissing, S. DeJong, S. M. Collins, and C. R. McKay, "Segmentation of intravascular ultrasound images: A knowledge-based approach," *IEEE Trans. Med. Imag.*, vol. 14, pp. 719–732, Aug. 1995.
- [17] M. Sonka, X. Zhang, S. C. DeJong, S. M. Collins, and C. R. McKay, "Automated detection of coronary wall and plaque borders in ECG-gated intravascular ultrasound pullback sequences (abstract)," *Circ.*, vol. 94, pp. 1–653, 1996.
- [18] R. T. Lee, H. M. Loree, G. C. Cheng, E. H. Liegerman, N. Jaramillo, and F. J. Schoen, "Computational structural analysis based on intravascular ultrasound imaging before *in vitro* angioplasty: Prediction of plaque fracture locations," *J. Amer. Coll. Cardiol.*, vol. 21, pp. 777–782, 1993.
- [19] S. P. Wiet, M. J. Vonesh, M. J. Waligora, B. J. Kane, and D. D. McPherson, "The effect of vascular curvature on three dimensional reconstruction of intravascular ultrasound images," *Ann. Biomed. Eng.*, vol. 24, pp. 695–701, 1996.

- [20] G. P. M. Prause, S. C. DeJong, C. R. McKay, and M. Sonka, "Geometrically correct 3-D reconstruction of tortuous coronary arteries: Fusion of biplane coronary angiography and intravascular ultrasound pullback imaging (abstract)," *Circ.*, vol. 94, pp. I-255, 1996.
- [21] D. Baumgart, M. Haude, J. Ge, G. Gorge, F. Liu, V. Shah, and R. Erbel, "Online integration of intravascular ultrasound images into angiographic images [letter]," *Cathet. Cardiovasc. Diagn.*, vol. 39, pp. 328-329, 1996.
- [22] C. Pellot, I. Bloch, A. Herment, and F. Sureda, "An attempt to 3-D reconstruct vessel morphology from X-ray projections and intravascular ultrasound modeling and fusion," *Computerized Med. Imag., Graph.*, vol. 20, pp. 141-151, 1996.
- [23] G. P. M. Prause, S. DeJong, C. R. McKay, and M. Sonka, "Toward a geometrically correct 3-D reconstruction of tortuous coronary arteries based on biplane angiography and intravascular ultrasound," *Int. J. Card. Imag.*, vol. 13, pp. 451-462, 1997.
- [24] G. S. Mintz, A. D. Pichard, J. J. Popma, K. M. Kent, L. F. Satler, T. A. Bucher, and M. B. Leon, "Determinants and correlates of target lesion calcium in coronary artery disease: A clinical, angiographic and intravascular ultrasound study," *J. Amer. Coll. Cardiol.*, vol. 29, pp. 268-274, 1997.
- [25] Q. Rasheed, R. Nair, H. Sheehan, and J. M. Hodgson, "Correlation of intracoronary ultrasound plaque characteristics in atherosclerotic coronary artery disease patients with clinical variables," *Amer. J. Cardiol.*, vol. 73, pp. 753-758, 1994.
- [26] Q. Rasheed, P. J. Dhawale, J. Anderson, and J. M. Hodgson, "Intracoronary ultrasound-defined plaque composition: Computer-aided plaque characterization and correlation with histologic samples obtained during directional coronary atherectomy," *Amer. Heart J.*, vol. 129, pp. 631-637, 1995.
- [27] P. R. Liebson and L. W. Klein, "Intravascular ultrasound in coronary atherosclerosis: A new approach to clinical assessment," *Amer. Heart J.*, vol. 123, pp. 1643-1660, 1991.
- [28] C. D. Mario, S. H. K. The, S. Madretsma, R. J. van Suylen, R. Wilson, N. Bom, P. W. Serruys, E. J. Gussenhoven, and J. R. T. C. Roelandt, "Detection and characterization of vascular lesions by intravascular ultrasound: An *in-vitro* study correlated with histology," *J. Amer. Soc. Echocardiogr.*, vol. 5, pp. 135-146, 1992.
- [29] E. Picano, L. Landini, M. P. Urbani, A. Mazzarisi, M. Paterni, and A. M. Mazzone, "Ultrasound tissue characterization techniques in evaluating plaque structure," *Amer. J. Cardiac Imag.*, vol. 8, pp. 123-128, 1994.
- [30] P. J. de Feyter, C. D. Mario, and P. W. Serruys, *Quantitative Coronary Imaging*. Rotterdam, The Netherlands: Barjeste Meeuwes, 1995.
- [31] L. S. Wilson, M. L. Neale, H. E. Talhami, and M. Appleberg, "Preliminary results from attenuation-slope mapping of plaque using intravascular ultrasound," *Ultrasound in Med., Biol.*, vol. 20, pp. 529-542, 1994.
- [32] S. L. Bridal, P. Fornes, P. Bruneval, and G. Berger, "Correlation of ultrasonic attenuation (30 to 50 MHz) and constituents of atherosclerotic plaque," *Ultrasound in Med., Biol.*, vol. 23, pp. 691-703, 1997.
- [33] G. Belcaro, G. Laurora, M. R. Cesarone, M. T. D. Sanctis, L. Incandela, E. Fascetti, G. Geroulakos, G. Ramaswami, A. Pierangeli, and A. N. Nicolaidis, "Ultrasonic classification of carotid plaques causing less than 60% stenosis according to ultrasound morphology and events," *J. Cardiovasc. Surg.*, vol. 34, pp. 287-294, 1993.
- [34] A. M. Mazzone, M. P. Urbani, E. Picano, M. Paterni, E. Borgatti, A. D. Fabritiis, and L. Landini, "In vivo ultrasonic parametric imaging of carotid atherosclerotic plaque by videodensitometric technique," *Angiol.*, vol. 46, pp. 663-672, 1995.
- [35] B. Griewing, U. Schminke, C. Morgenstern, M. L. Walker, and C. Kessler, "Three-dimensional ultrasound angiography (power mode) for the quantification of carotid artery atherosclerosis," *J. Neuroimag.*, vol. 7, pp. 40-45, 1997.
- [36] T. Noritomi, B. Sigel, V. Swami, J. Justin, V. Gahtan, X. Chen, E. J. Feleppa, A. B. Roberts, and K. Shirouzu, "Carotid plaque typing by multiple-parameter ultrasonic tissue characterization," *Ultrasound in Med., Biol.*, vol. 23, pp. 643-650, 1997.
- [37] B. J. Kimura, V. Bhargava, and A. N. DeMaria, "Value and limitations of intravascular ultrasound imaging in characterizing coronary atherosclerotic plaque," *Amer. Heart J.*, vol. 130, pp. 386-396, 1995.
- [38] S. A. Wickline, J. G. Miller, D. Rechia, A. M. Sharkey, L. Bridal, and D. Christy, "Beyond intravascular imaging: Quantitative ultrasonic tissue characterization of vascular pathology," in *Proc. IEEE Ultrasonics Symp.*, 1994, pp. 1589-1597.
- [39] M. S. Bissing, S. DeJong, P. Thomas, K. Spencer, and C. R. McKay, "Identification of eccentric lesions and lipid laden plaques by IVUS: Validation by quantitative histology in fresh cadaveric hearts (abstract)," *Circ.*, vol. 90, pp. I-551, 1994.
- [40] M. Sonka, V. Hlavac, and R. Boyle, *Image Processing, Analysis, and Machine Vision*, 2nd ed. Pacific Grove, CA: PWS, 1998; 1st ed. London, U.K.: Chapman and Hall, 1993.
- [41] M. M. Galloway, "Texture classification using gray level run length," *Comp. Graphics and Image Proc.*, vol. 4, pp. 172-179, 1975.
- [42] A. Gisolfi, S. Vitulano, and A. Cacace, "Texture and structure," in *Advances in Image Processing and Pattern Recognition*, V. Cappellini and R. Marconi, Eds. Amsterdam, The Netherlands: North Holland, pp. 179-183, 1986.
- [43] C. M. Wu, Y. C. Chen, and K. S. Hsieh, "Texture features for classification of ultrasonic liver images," *IEEE Trans. Med. Imag.*, vol. 11, pp. 141-152, 1992.
- [44] H. C. Andrews, *Introduction to Mathematical Techniques in Pattern Recognition*. New York: Wiley, 1972.
- [45] R. J. Schalkoff, *Pattern Recognition: Statistical, Structural and Neural Approaches*. New York: Wiley, 1992.
- [46] P. A. Lachenbruch, "An almost unbiased method for obtaining confidence intervals for the probability of misclassification in discrimination analysis," *Biometrics*, vol. 23, pp. 639-645, 1967.
- [47] P. J. Fitzgerald, T. A. Ports, and P. G. Yock, "Contribution of localized calcium deposits to dissection after angioplasty. An observational study using intravascular ultrasound," *Circ.*, vol. 86, pp. 64-70, 1992.
- [48] G. S. Mintz, B. N. Potkin, G. Keren, L. F. Satler, A. D. Pichard, K. M. Kent, J. J. Popma, and M. B. Leon, "Intravascular ultrasound evaluation of the effect of rotational atherectomy in obstructive atherosclerotic coronary artery disease," *Circ.*, vol. 86, pp. 1383-1393, 1992.
- [49] J. Honye, D. J. Mahon, C. J. White, S. R. Ramee, J. B. Wallis, A. Al-Zarka, and J. M. Tobis, "Morphological effects of coronary balloon angioplasty *in vivo* assessed by intravascular ultrasound imaging," *Circ.*, vol. 85, pp. 1012-1025, 1992.